Investigation of mechanical properties and temperature distribution of friction stir welded joint of 2024 and AA7075

Nisar Ahmad Bhat, Sorabh Gupta, Vikas Nandal

Department of Mechanical Engineering Geeta Engineering College, Naultha, Panipat, India

Abstract

The scope of this investigation is to evaluate the effect of joining parameters on the mechanical properties, microstructural features and material flow of dissimilar aluminium alloys of AA2024-and AA7075-T6 sheets) joints produced by friction stir welding. Mechanical performance has been investigated in terms of hardness and tensile testing. Material flow using the stop action technique has also been investigated in order to understand the main features of the mixing process. The maximum tensile strength 262.06MPa was achieved at the welding speed of 40mm/min with tool rotational speed 120 rpm and tilt angle 0°. The fractured locations of the FSW welded joint of AA2024 and AA7075 at different traverse speed were found in the heat affected zone. The hardness of stir zone was increased when the traverse speed increases up to 40mm/min after that hardness value decreases. The highest value of hardness(154HV) was observed in the stir zone at 40mm/min whereas minimum hardness (130HV) was found in the stir zone at 25mm/min. It was also seen that the peak temperature decreases with increase in traverse speed. ©2020 ijrei.com. All rights reserved

Keywords: Aluminum alloys, Zinc percentage, Tensile strength, Hardness

1. Introduction

Friction stir welding (FSW) is a relatively new solid-state joining technique which is widely adopted in different industry fields to join different metallic alloys that are hard to weld by conventional fusion welding. FSW is a highly complex process comprising several highly coupled physical phenomena. The complex geometry of some kinds of joints and their three-dimensional nature make it difficult to develop an overall system of governing equations for theoretical analyzing the behavior of the friction stir welded joints. The experiments are often time-consuming and costly. To overcome these problems, numerical analysis has frequently been used since the 2000s. The heat and mass transfer is mainly influenced by material properties as well as welding variables including the rotational and transverse tool speed. However, the joining takes place by extrusion and forging of the metal at high strain rates [1]. The maximum temperature ranges from 80 to 90% of the melting temperature of the welding material at the interface between the tool and the work-piece. However, 20% of the total heat is attributed to the pin and the addition of heat due to the pin has little effect on the thermal profile [2]. The nature of heat transfers and heat generation rate,

and flow of plasticized material is primarily affected by tool geometry, traverse movement of the tool, applied torque and thermo- mechanical condition experienced by the tool [3]**.** A dimensionless correlation has been developed based on Buckingham's pi-theorem. The relationship can also be used for the selection of welding conditions to prevent melting of the work-piece during FSW. The correlation includes thermal properties of the material and the tool, the area of the tool shoulder and the rotational and translation speeds of the tool [4]. The thermo-mechanical simulation of friction stir welding can predict the transient temperature field, active stresses developed, forces in all the three dimensions and may be extended to determine the residual stress [5]. The shape of the tool pins also influences the flow of plasticized material and finally affects weld joint properties. The tool shoulder facilitates bulk material flow, whereas the pin aids a layer- by-layer material flow. A triangular tool pin increases the material flow compared with a cylindrical pin [6]. The effect of friction stir processing on TIG welded joint have been analyzed and they observed mechanical properties and heat transfer of TIG+FSP welded joint. The mechanical properties of TIG+FSP welded joint were observed better than TIG welded joints. [7-13]. The effect of the mass scaling factor

on the temperature field during the plunge stage in FSW was analyzed. The transfer processes were described by the system of diffusion and motion equations including contact detection and interaction solutions for particles integrated over time. Modeling of the tool/work-piece interface included both the mixing of the oxide particles into the subsurface layer during hot rolling of aluminum and heat generation during FSW [14]. The numerical model is continuum solid mechanics-based, fully thermo-mechanically coupled and has successfully simulated the FSW process including plunging, dwelling and welding stages. The equivalent load method based on the inherent strain approach was suggested as an efficient welding deformation and residual stress analysis method for large scale FSW structures of aluminum alloy Al6061-T6 sheet metal. The results show fairly good agreements with those of existing FE analysis as well as the FSW experiments [15]. The distribution of temperature, strain, stress and metal flow state of the specimen were obtained and the defects were forecast for the FSW process. The results showed that the temperature distribution of the workpiece is asymmetrical; strain distribution is not uniform throughout the thickness of the specimen, and severe plastic deformation exists in the welding zone [16]. The tool rotational speed, traverse speed, and tilt angle were basic parameters during the FSW process that have a substantial influence on the temperature distribution of the workpiece [17, 18], the mechanical and metallurgical characterization of the welded joint [19] and material flow behavior [20]. The progress in numerical temperature simulations of FSW has been achieved by researchers and numerical analysis has found widespread application [21]. In this work, the mechanical properties of FSW welded joint of AA2024 and AA7075 has been investigated and develop and validate a three dimensional thermo-mechanical model of friction stir welding process and predict the variation of the temperature distribution of the welded joint of dissimilar aluminum alloy of AA2024 and Aa7075.

2. Materials and Method

In this work, the thermo-mechanical model was developed using the finite element method using ANSYS 14. In order to validate the developed model, the output of the model was correlated with the published results. Once developed, the thermo-mechanical model was used to simulate the process. The model was then extrapolated to perform parametric studies in order to investigate the effects of various process parameters on temperature distribution and residual stress in the work-piece. The next step was to construct surrogate models using the data generated by the thermo-mechanical model and evaluate the temperature distribution and heat flux of the friction stir welded plate. The friction stir welding of the AA2024 and AA7075 aluminum alloy was performed using a tool with a 4 mm diameter and 5.5 mm length circular threaded pin and having a shoulder diameter of 19 mm. The optimal welding speed depends on various factor.
Aluminium alloy of AA7075 and AA2024 are selected to fabricate dissimilar joints using friction stir welding (FSW). The length, width and thickness of both the alloy plates are chosen as 120, 40 and 6.3 mm respectively. The chemical composition of AA7075 and AA2024 are given in table 1.

Table 1: Chemical composition of Aluminum alloy

Al- alloy	Si	Fe	Cu	Mn	Mg	Cr	Zn	Al
2024	0.4	0.45	4.2	0.6	1.4	0.12	0.24	Bal
7075	0.2	0.1	1.3	0.03	2.7	0.2	5.78	Bal

The processing parameters of friction stir welding of dissimilar aluminum alloy AA2024 and AA7075 as shown in table 2.

Table 2: Processing parameter for friction stir welding

Sample No	Tilt angle	Tool rotational speed (rpm)	Welding Speed (mm/min)
1			25
2			30
3	0°	1200	35
4			40
5			45

2.1 Governing Equation [22]

The continuity equation for incompressible single-phase flow in index notation for i = 1, 2 and 3, representing the x, y and z directions, respectively is given by

$$\frac{\partial u_i}{\partial x_i} = 0 \tag{1}$$

where u is the velocity of plastic flow. The steady single phase momentum conservation equations with reference [23] to a coordinate system attached to the heat source in index form may be represented as

$$\rho \frac{\partial u_I u_j}{\partial x_i} = -\frac{\partial P}{\partial x_j} + \frac{\partial}{\partial x_I}\left(\mu \frac{\partial U_j}{\partial x_i} + \mu \frac{\partial U_i}{\partial x_j}\right) - \rho\, U_1\left(\frac{\partial U_j}{\partial x_I}\right) \tag{2}$$

where ρ is the density, μ is the non-Newtonian viscosity, U_1 is the welding velocity and *p* is the pressure. The constitutive equations used here for viscosity calculation have been used for hot-working processes, particularly extrusion. Friction stir welding involves transfer of plasticized material from the front to the back of the tool pin as the tool traverses along the joint. It is basically an extrusion process followed by forging which joins the plates. Therefore, it is appropriate to use these equations for FSW. The calculation of viscosity requires local values of strain rate and temperature [23].

$$\sigma_e = \frac{1}{\alpha} sinh^{-1}\left[\left(\frac{Z}{A}\right)^{1/n}\right] \tag{3}$$

where A, a and n are material constants and Z is the Zener–Hollomon parameter. Parameter A is a function of the carbon concentration in C–Mn-steel, while a and n depend on the temperature, T, as indicated below [23].

$$A = 1.80 \times 10^6 + 1.74 \times 10^8 \,(\%C) - 6.5 \times 10^7 \,(\%C)^2 \tag{4}$$
$$\alpha = 1.07 + 1.70 \times 10^{-4}\,T - 2.81 \times 10^{-7}\,T^2 \tag{5}$$
$$n = 0.2 + 3.966 \times 10^{-4}\,T \tag{6}$$

Z, the Zener–Hollomon parameter, represents the temperature compensated effective strain rate and is given by

$$Z = \varepsilon \exp\left(\frac{Q}{RT}\right) \tag{7}$$

Here Q is the temperature independent activation energy, R is gas constant and ε is the effective strain rate, given by

$$\varepsilon = \left(\frac{2}{3}\varepsilon_{ij}\varepsilon_{ij}\right)^{1/2} \tag{8}$$

where ε_{ij} is the strain rate tensor, defined as

$$\varepsilon_{ij} = \frac{1}{2}\left(\frac{\partial u_i}{\partial x_j} + \frac{\partial u_j}{\partial x_i}\right) \tag{9}$$

Finally, viscosity can be determined from flow stress and effective strain rate using Perzyna's visco-plasticity model [24].

$$\mu = \frac{\sigma_e}{3\varepsilon} \tag{10}$$

The above formulation indicates that dynamic viscosity is a strong function of local strain rate and temperature. The strain rate is the more dominant factor for the conditions typical of FSW. For the same temperature and strain rate, the viscosity values are about one order of magnitude higher than those reported for the FSW of aluminum. The steady thermal energy conservation equation is given by

$$\rho C_p \frac{\partial(u_i T)}{\partial x_i} = -\rho C_p U_I \frac{\partial T}{\partial x_i} + \frac{\partial}{\partial x_i}\left(k\frac{\partial T}{\partial x_i}\right) + S_i + S_b \tag{11}$$

Where C_p is the specific heat and k is the thermal conductivity of the workpiece/tool. The term S_i represents the source term due to interfacial heat generation rate per unit volume at the tool pin–workpiece interface and S_b is the heat generation rate due to plastic deformation in the work-piece away from the interface. The heat generated at the interface between vertical and horizontal surface of the tool pin and the work-piece, Si, may be defined as:

$$S_i = [(1-\delta)\eta\tau + \delta\mu_f P_N] (\omega r - U_I \sin\theta)\frac{A_r}{V} \tag{12}$$

where Ar is any small area on the tool pinwork-piece interface, r is the radial distance of the center of the area from the tool axis, *V* is the control-volume enclosing the area A_r, τ is the maximum shear stress at yielding, θ is the angle with the negative x-axis in the counter-clockwise direction, η is the mechanical efficiency, i.e. the amount of mechanical energy converted to heat energy. δ denotes the spatially variable fractional slip between the tool and the work-piece interface, μ_f is the spatially variable coefficient of friction, ω is the angular velocity and P_N is the normal pressure on the surface, which is equal to P_V for the work-piece area in contact with the vertical surface of the pin and equal to P_H for area below the horizontal surface of the tool. The velocity ($\omega r - U_I \sin\theta$) represents the local velocity of a point on tool with the origin fixed at the tool axis. A 50% mechanical efficiency was assumed guided by the range of the previous work in FSW [25]. In Eq. (12) the radial pressure is much smaller than the axial pressure and the value of P_V has been assumed to be

zero. When δ is 0, full sticking is indicated and all the heat is generated by plastic deformation, while heat is generated only by friction when $\delta = 1$.

During FSW, mixing is not atomic, as evident from the previous research on dissimilar metal joining [26-27]. Here grains are deformed but efficient mixing of atoms does not occur. A rigorous calculation of heat generation due to viscous dissipation of momentum is difficult. However, previous research has shown that the heat generation due to viscous dissipation is small, of the order of only 4.4% of the total heat generation for the FSW of aluminum alloy [28]. A rough estimate of the viscous dissipation of momentum per unit volume, S_b has been calculated $f_m\mu\varphi$, where φ is given by [27]. fm is an arbitrary constant that indicates the extent of atomic mixing in the system. The value of f_m will tend to 1 for a well-mixed system in the atomic scale. In systems where the grains remain largely intact, the value of f_m will be very small. Here, a value of 0.05 was used because this value resulted in the viscous dissipation being about 4% of the total heat generation for the welding conditions investigated.

$$\Phi = 2\left[\left(\frac{\partial u_1}{\partial x_1}\right)^2 + \left(\frac{\partial u_2}{\partial x_2}\right)^2 + \left(\frac{\partial u_3}{\partial x_3}\right)^2\right] + \left(\frac{\partial u_1}{\partial x_2} + \frac{\partial u_2}{\partial x_1}\right)^2 +$$
$$\left(\frac{\partial u_1}{\partial x_3} + \frac{\partial u_3}{\partial x_1}\right)^2 + \left(\frac{\partial u_3}{\partial x_2} + \frac{\partial u_2}{\partial x_3}\right)^2 \tag{13}$$

2.2 Boundary conditions

When the work-piece top surface away from the tool shoulder edge, the boundary condition for heat exchange involves both convection and radiation heat transfer. However, at the sides and the bottom surface of the work-piece, the boundary condition for heat exchange involves only convection heat transfer. The heat generation rate at the interface between tool and the work-piece can be given by
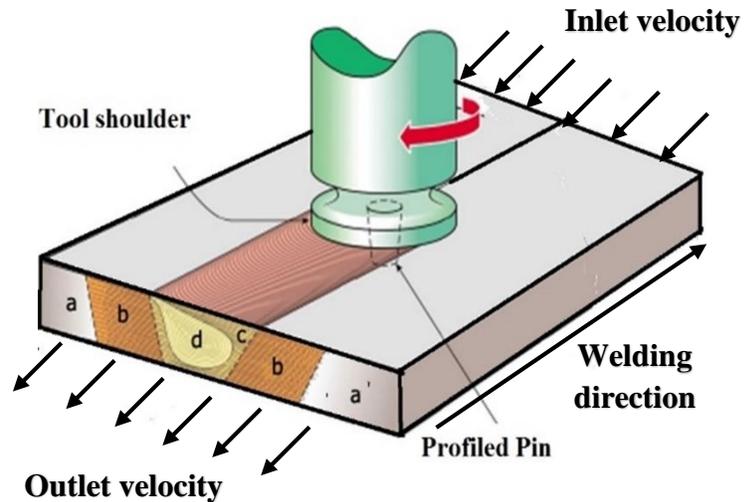

Figure 1: Boundary condition of friction stir welding

$$f = \frac{J_W}{J_T} = \frac{\sqrt{(k_\rho C_P)_W}}{\sqrt{(k_\rho C_P)_T}} \tag{14}$$

Where T and W denote the tool and work piece respectively. The heat flux continuity on the shoulder interface yields

$$k \left.\frac{\partial T}{\partial z}\right|_{top} = \frac{J_w}{J_w + J_T} q_I \text{ in the range of } R_P \leq r \leq R_s \quad (15)$$

Where J_w and J_T were the heat conducted to the work-piece and tool respectively

$$J = \sqrt{k\rho\, C_p} \quad (16)$$

Where Cp was heat capacity, ρ and K were density and thermal conductivity respectively

The total heat generation rate may be written as

$$q_I = [\eta\,(1 - \delta)\,\tau + \delta.\mu_{f.}P_H]\,(\omega.r - U_I\sin\theta) \quad (17)$$

The heat transfer coefficient may be calculated as

$$k \left.\frac{\partial T}{\partial z}\right|_{bottom} = h_b\,(T\text{-}T_a) \quad (18)$$

Value of h_b can be calculated as

$$h_b = h_{b0}\,(T\text{-}T_a)^{0.25} \quad (19)$$

The heat transfer due to radiation and convection was written as

$$k \left.\frac{\partial T}{\partial z}\right|_{top} = h_t\,(T\text{-}T_a) + \sigma\,\varepsilon^I(T^4\text{-}T_a^4) \quad (20)$$

In this model, the computational region was considered as a single-phase visco-plastic non-Newtonian fluid and the FSW tool was considered as rotating in a fixed position. The material flows into the computational domain from the inlet velocity and out from outlet velocity at the welding speed (traverse speed). Top, bottom, and side surfaces of the work-pieces were considered equivalent to the wall surface, having the same velocity as welding speed but opposite in direction.

Velocity at the tool pin periphery have been defined in terms of tool translation velocity and the tool pin angular velocity

$$\left.\begin{array}{l} u = (1 - \delta)(\omega R_P \sin\theta - U1) \\ v = (1 - \delta)\omega R_P \cos\theta \\ w = k\,\frac{\omega}{2\pi} R_P \end{array}\right\} \text{ in the range } R_P \leq r \leq R_S$$

$$(21)$$

Similarly, at the shoulder contact, the velocity boundary condition may be written as

$$\left.\begin{array}{l} u = (1 - \delta)(\omega r \sin\theta - U1) \\ v = (1 - \delta)\omega r \cos\theta \end{array}\right\} \text{ in the range } R_P \leq r \leq R_S$$

$$(22)$$

3. Results and Discussion

3.1 Tensile strength

Fig. 2, illustrate the stress strain diagram of the FSW butt welded

joint of dissimilar aluminum alloys of AA2024 and AA7075 at various traverse speed (25, 30, 35, 40, 45 mm/min) for the constant rotational speed (1200 rpm) and tilt angle (0º). Its cleared that all the welded joints show lower yield strength, ultimate tensile strength than those of base material. The change of traverse speed has a significant effect on the tensile strength of the welded joints. When the traverse speed increases tensile strength also increases up to 40 mm/min, after that decreases as shown in table 3. The tensile strength and fractured locations of the friction stir welded joint of AA2024 and AA7075 at different traverse speed are summarized in table 3. When the aluminum alloy AA075 was located on the advancing side (A.S), the tensile strength of welded joints was increased.
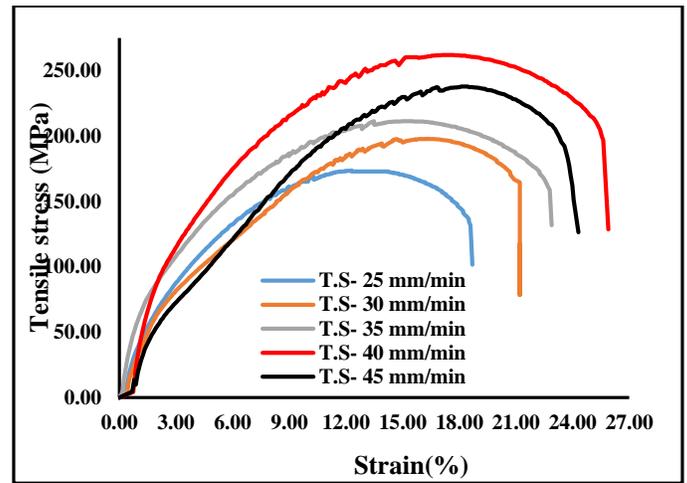

Figure 2: Stress strain diagram of FSW welded joint of AA2024 and AA7075 with different processing parameters

The maximum tensile strength 262.06 MPa was archived at the welding speed of 40 mm/min with tool rotational speed 120 rpm and tilt angle 0°. The kissing bond at the root of the joint was found when the aluminum alloy AA7075 was located on retreating side. When the welding speed was increased, the tensile strength was reduced due to the formation of kissing bond and pores in the stir zone. The enhancement of the tensile strength of the welded joints observed when AA7075 was located on the advancing side and the fractured location was observed at the heat affected zone of AA2024 [29], whereas some specimens was fractured at the stir zone of the welded joints. Therefore, the tensile strength of FSW welded joint of AA2024 and AA7075 were depended on the hardness and welding defects of the joints. When the welded joints are free from defect, the tensile strength was increased and the fractured occurred in the heat affected zone on the minimum hardness side material.

Table 3: Tensile strength of FSW welded joint of AA2024 and AA7075

Processing Parameter			Mean Tensile Strength (MPa)	Mean Strain (%)
Feed rate (mm/min)	TRS (rpm)	Tilt angle		
25			173.1	18.7
30			197.8	21.2
35	1200	0	211.3	22.9
40			262.06	25.9
45			237.8	24.3

3.2 Micro-hardness

Fig. 3 shows the variation of micro-hardness profile from the weld center line and 41 observations have been taken from the 1st base metal (AA2024) to 2nd base metal (AA7075) as shown in fig.3. A lower hardness values were observed on both advancing and retreating side in the weld as compare to base material. This is due to there-precipitation of strengthening precipitates, dissolution and coarsening caused by thermal cycle [30]. The micro-hardness distribution profile was heterogeneous in the nugget zone consisting of AA7075 and AA2024 base material. It can be observed that the all points show the asymmetric hardness distribution profile due to the asymmetrical material flow and heat generation caused by the friction stir welding tool, which was typical for the dissimilar aluminum alloy welded joints

The micro-hardness measurements were performed across the stir zone (SZ), thermo-mechanically affected zone (TMAZ), heat affected zone (HAZ) and base material. Fig.3 shows the micro-hardness profiles of FSW welded joint at traverse speed of 25, 30, 35, 40 and 45 mm/min with constant rotational speed of 1200 rpm with constant tilt angle 0°. The heat affected zone of welded joints were expected to have lowest hardness in the weld zone due to dissolution of the precipitation phase in that zone. The increase in the hardness at the stir zone was also reported in the friction stir welding of other precipitation hardened alloys [31-32]. The micro-hardness values are less momentous in affecting the mechanical properties of the welded joint, because processing parameter (tool rotation speed, current, feed rate etc.) have more influencing factor over the hardness value [13]. The micro hardness values at the middle and bottom of the welded joint detected the major effect, because the grain size and micro-hardness number were changed due to solidification sequence and cooling rate of the weldment.
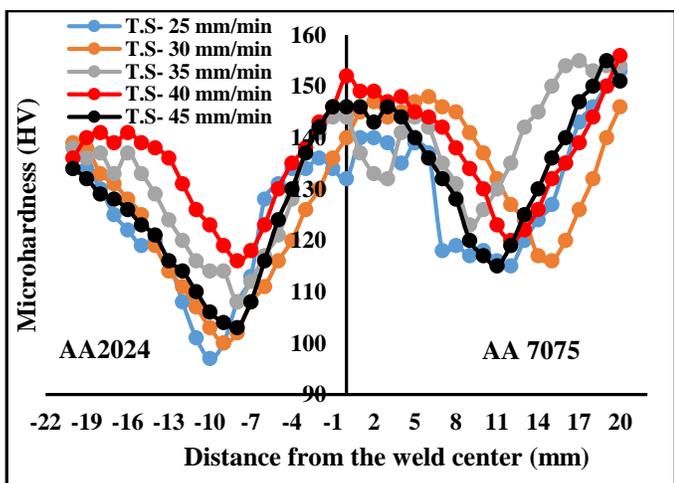

Figure 3: Variation of micro-hardness of welded joint of dissimilar aluminum alloy of AA2024 and AA7075

The microhardness number also play a very important role to recognizing the metallurgical phase. Due to coarsening of the hardening phases in TMAZ region, slightly decreases in the hardness observed in the TMAZ. The lowest hardness was observed in HAZ region on both side of the base material. The

hardness of stir zone was increased when the traverse speed increases up to 40 mm/min after that hardness value decreases. The highest value of hardness (154 HV) was observed in the stir zone at 40 mm/min whereas minimum hardness (130 HV) was found in the stir zone at 25 mm/min.

3.3 Residual stress

The residual stress at the welded region is one of the most significant parameters for analyzing the mechanical properties of the welded joint. The tensile stress was carried by imposing tensile loading, compressive residual stress may be effective in enhance the mechanical properties of the welded joint. The residual stress in the nugget zone and the formation of compressive residual stress in the TMAZ contribute to enhancement of the mechanical properties of the FSW welded joint [33]. The ultimate tensile strength and hardness may be improved by imposing compressive residual to the FSW welded region. The highest tensile residual stress was found along the welded line at the edge of weld in advancing side. This high residual stresses achieved on the advancing side of the FSW welded region are associated with the high traverse speed of the tool [34].
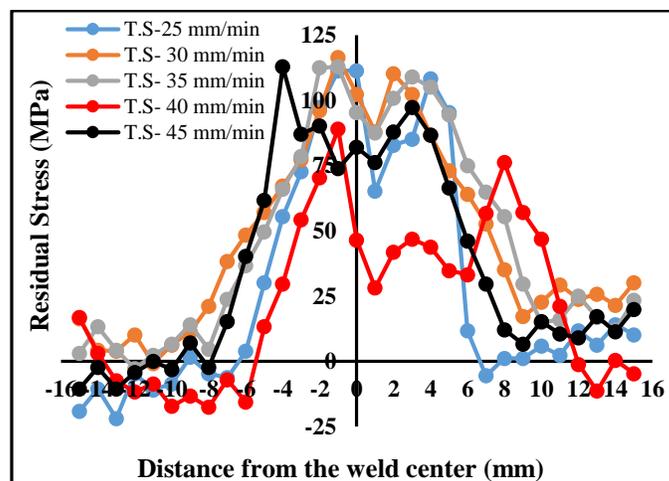

Figure 4: Variation of residual stress distribution of welded joint of AA2024 and AA7075

Residual stress distribution profile in the transverse direction of the FSW welded joint of dissimilar aluminum alloy of AA2024 and AA7075 as shown in fig.4, where it can be observed that the base material AA2024 and AA7075 has homogenous residual stresses from -18 to -12 MPa at base metal AA2024 and 10-15 MPa at second base metal AA7075. The transverse tensile residual stress peak at nugget zone decreased when traverse speed increased from 25 to 40 mm/min after that residual stress was increased. The maximum tensile residual stress (111 MPa) in the nugget zone was observed at traverse speed 25 mm/min with tool rotational 1200 rpm and tilt angle 1°, whereas minimum tensile residual stress (46.48 MPa) at nugget zone was observed at traverse speed of 40 mm/min. The base material AA2024 and AA7075 has a homogenous residual stress distribution. The friction stir welding is an asymmetric thermo-mechanical

process, it was observed that both advancing side and retreating side would have different residual stress. So, the residual stress distributions are a function of the traverse speed and tool rotational speed [35]. There are many which affect the residual stress, such as modulus of elasticity, welding parameters, coefficient of thermal expansion and metal flow around the heat source. The transverse residual stresses show the tensile stress in the welded region and shifted compressive stress toward the base material on the both sides. The transverse residual stress was axisymmetric on both sides of the dissimilar aluminum alloy welded region as shown in fig.4. Generally, the longitudinal residual stresses, which are generated due to the contraction of the FSW weld during cooling, were symmetrical on both side of the weldment [36-37].

3.4 Temperature distribution

3.4.1 Validation of results

It was momentous to get the validated the numerical results which can be used to predict confident results for this study as shown in table 4. Usually, numerous simulation studies have been validated their models through the comparison of the temperature distribution. In this work, the measured temperature was recorded from ANSYS 14 corresponding to process parameters at tool rotation speed 1200 rpm, and traverse speed (25, 30, 35, 40, 45 mm/min). The present result was validated by Padmanaban et al [38] which gives a satisfactory amount of assurance in the fidelity of the simulation of welded joints.

Table 4: Validation of results

Traverse speed (mm/min)	Tool rotational speed (rpm)	Temperature (K)	
		Padmanaban et al [38]	Present value
20	1200	745	751

3.4.2 Temperature distribution of the FSW welded joint

During friction stir welding, the heat generation must be sufficient to soften the stir zone and mix the material very well. The computed temperature profile along the top surface of the base plate through the tool pin axis are shown in fig. 6.

The temperature contour on during the friction stir welding of AA2024 and AA7075 at various traverse speed (25, 30, 35, 40, 45 mm/min) with constant tool rotational speed 1200 rpm with tilt angle 0° are shown in fig.6. It was seen that the peak temperature decreases with increases in traverse speed as shown in fig.7. As the traverse speed increases from 25 to 45 mm/min, the temperature at nugget zone decreases from 751 to 703K. This reduction in temperature was due to the decreased dissipation of heat over a wider region and heat input per unit length of the base plate at the higher traverse speed. When the traverse speed is low, the material near to the rotating tool is subjected to higher temperatures. This increase in temperature, stirring material that was softened due to increased temperature thus reducing the force acting on the rotating tool. When the traverse speed was high, the material near to the tool subjected to low temperatures resulting in the tool stirring a comparatively harder material, increasing the

forces acting on the tool [39]. The higher temperature (751K) was observed at traverse speed of 25 mm/min whereas low temperature (703K) was observed at traverse speed of 45 mm/min.
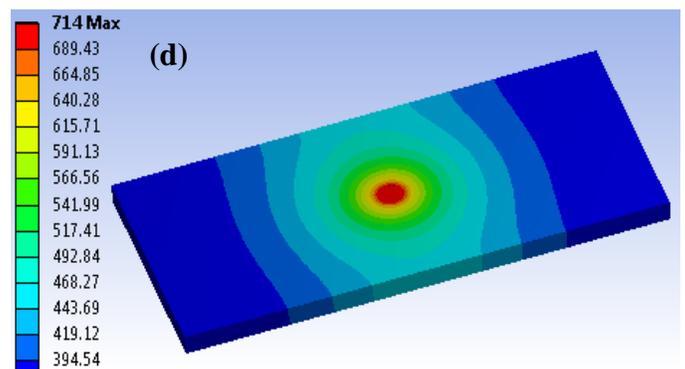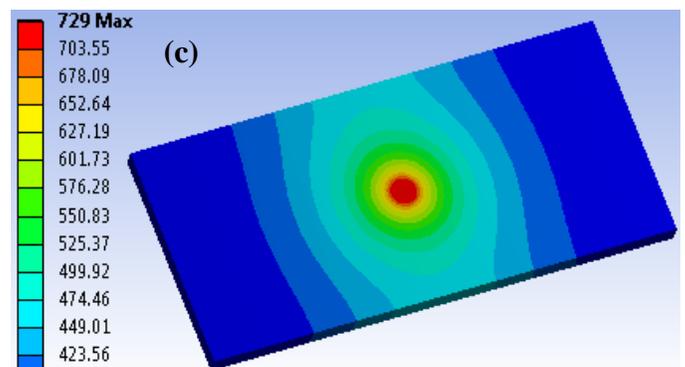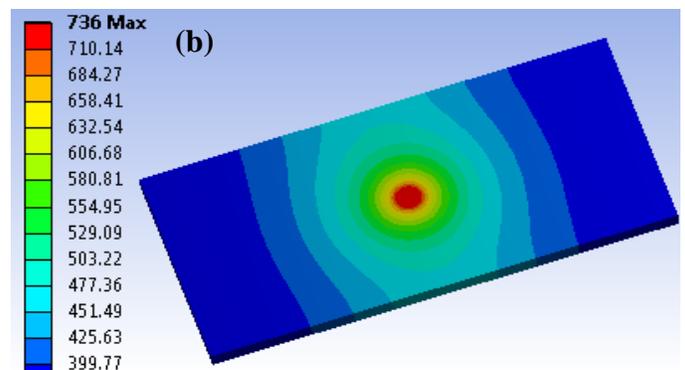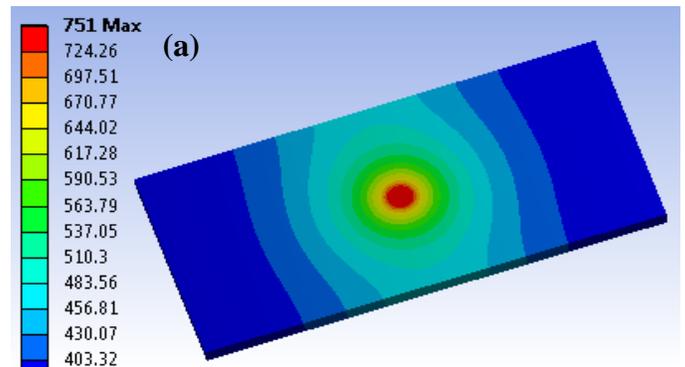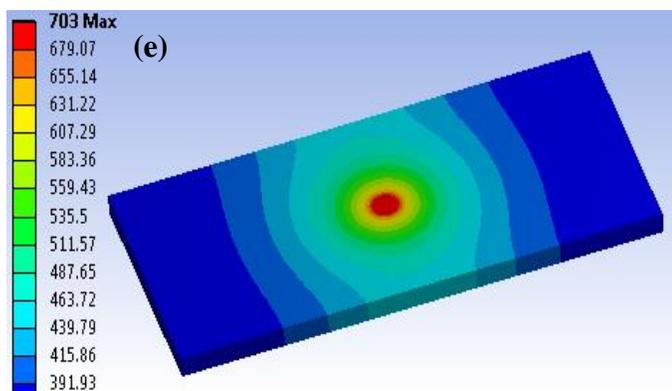
*Figure 6: Temperature distribution of friction stir welding of AA2024 and AA7075*
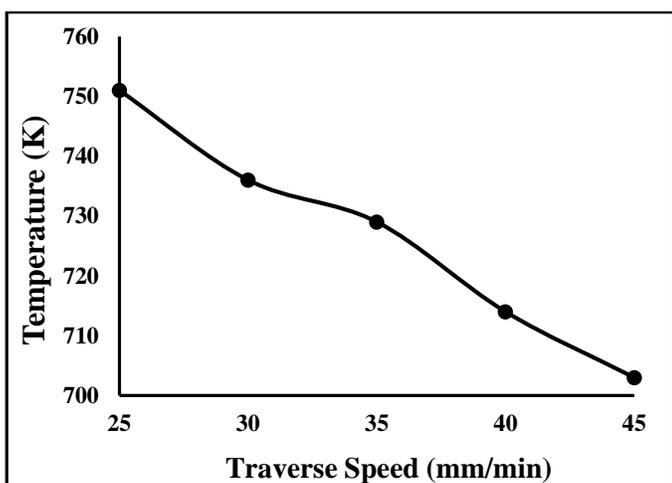
Figure 7: Variation of temperature at nugget zone and traverse speed of the FSW welded joint

4. Conclusions

The mechanical properties and the temperature distribution of friction stir welded joint of dissimilar aluminum alloys AA2024 and AA7075 has been investigated and following conclusion have been made.

- The maximum tensile strength 262.06 MPa was archived at the welding speed of 40 mm/min with tool rotational speed 120 rpm and tilt angle 0° and minimum tensile strength (171 MPa) was observed at 25 mm/min.
- The fractured locations of the friction stir welded joint of AA2024 and AA7075 at different traverse speed were found in the heat affected zone (HAZ).
- The tensile strength of FSW welded joint of AA2024 and AA7075 were depended on the hardness and welding defects of the joints. When the welded joints are free from defect, the tensile strength was increased and the fractured occurred in the heat affected zone on the minimum hardness side material.
- The hardness of stir zone was increased when the traverse speed increases up to 40 mm/min after that hardness value decreases. The highest value of hardness (154 HV) was observed in the stir zone at 40 mm/min whereas minimum hardness (130 HV) was found in the stir zone at 25 mm/min.

- The transverse tensile residual stress peak at nugget zone decreased when traverse speed increased from 25 to 40 mm/min after that residual stress was increased. The maximum tensile residual stress (111 MPa) in the nugget zone was observed at traverse speed 25 mm/min with tool rotational 1200 rpm and tilt angle 1°, whereas minimum tensile residual stress (46.48 MPa) was observed.
- The temperature contour on during the friction stir welding of AA2024 and AA7075 at various traverse speed (25, 30, 35, 40, 45 mm/min) with constant tool rotational speed 1200 rpm with tilt angle 0° are shown in fig.5. It was seen that the peak temperature decreases with increases in traverse speed

References

[1] Thomas,W.M.,Nicholas,E.D., Needham, J.C., Murch,M.G.,Smith, P. and Dawes,C.J.(1991),'Frictionstirbuttwelding',InternationalPatent Application No. PCT/GB92/02203.
[2] Chao, Y.J., Qi, X. and Tang, W. (2003), 'Heat transfer in friction stir welding- Experimental and numericalstudies', ASMETrans., 125: 138–45.
[3] Vijay Soundararajan, Srdja Zekovic, Radovan Kovacevic,Thermo-mechanical model with adaptive boundary conditions for friction stir welding of Al 6061, International Journal of Machine Tools & Manufacture 45 (2005) 1577–1587, Received 5 January 2005; accepted 15 February 2005,Available online 21 April 2005.
[4] Schmidt,H.,Hattel,J. andWert,J. (2004),'An analyticalmodelforthe heat generation in frictionstir welding', Model.Simul. Mater. Sci. Eng., 12: 143–57.
[5] Reynolds AP, Tang W, Khandkar Z, Khan JA, Lindner K. Relationships between weld parameters, hardness distribution and temperature history in alloy 7050 friction stir welds. Sci Technol Weld Join2005;10:190–9.
[6] Elangovan,K. and Balasubramanian, V. (2007), 'Influences of pin profile and rotational speed of the tool on the formation of frictionstir processingzone in AA2219 aluminium alloy', Mater. Sci. Eng. A, 459: 7–18.
[7] Husain Mehdi, R.S Mishra (2016), Mechanical Properties and Microstructure Studies in Friction Stir Welding (FSW)Joints of Dissimilar Alloy-A Review, Journal of Achievements of Materials and Manufacturing Engineering , vol-77, issue1, pp 31-40.
[8] Husain Mehdi, R.S. Mishra (2019), Analysis of Material Flow and Heat Transfer in Reverse Dual Rotation Friction Stir Welding: A Review, International Journal of Steel Structure, vol-19, issue-2, pp 422-434.
[9] Husain Mehdi, R.S. Mishra (2019), Study of the influence of friction stir processing on tungsten inert gas welding of different aluminum alloy, SN Applied Sciences, vol-1, issue-7, 712.
[10] Husain Mehdi, R.S. Mishra (2020), Investigation of mechanical properties and heat transfer of welded joint of AA6061 and AA7075 using TIG+FSP welding approach, Journal of Advanced Joining Processes, vol-1, issue-1, 100003.
[11] Husain Mehdi, R.S. Mishra (2020), Effect of Friction Stir Processing on Microstructure and Mechanical Properties of TIG Welded Joint of AA6061 and AA7075, Metallography, Microstructure, and Analysis, vol-9, 403-418. https://doi.org/10.1007/s13632-020-00640-7.
[12] Husain Mehdi, R.S. Mishra (2020), Effect of friction stir processing on mechanical properties and heat transfer of TIG-welded joint of AA6061 and AA7075, Defence Technology. https://doi.org/10.1016/j.dt.2020.04.014.
[13] Husain Mehdi, R.S. Mishra (2020), Influence of friction stir processing on weld temperature distribution and mechanical properties of TIG welded joint of AA6061 and AA7075 Transactions of the Indian Institute of Metals, vol-73, 1773-1788.
[14] Li WY,YuM,Li JL. Effects ofmass scaling factor on the plunge stage of friction stir welding. Trans Chin Weld Inst 2010;31:1–4.
[15] Jang CD, Jang YJ. Welding deformation analysis of friction stir welded aluminum alloy structures using equivalent load method based on inherent strain. In:Proceedings of the international offshore and polar engineering conference, vol.4; 2010. pp.290–297.

[16] Zhou MZ, Lei DG, Liang N, Yang JH. 3Dcoupled thermo-mechanical visco-plastic finite element simulation of friction stir welding process. Trans Chin Weld Inst 2010;31:5–9.

[17] Abnar B, Kazeminezhad M, Kokabi A H. Effects of heat input in friction stir welding on microstructure and mechanical properties of AA3003-H18 plates [J]. Transactions of Nonferrous Metals Society of China, 2015, 25(7): 2147−2155.

[18] Dawood H I, Mohammed K S, Rahmat A, Uday M B. Effect of small tool pin profiles on microstructures and mechanical properties of 6061 aluminum alloy by friction stir welding [J]. Transactions of Nonferrous Metals Society of China, 2015, 25(9): 2856−2865.

[19] Hejazi I, Mirsalehi S E. Mechanical and metallurgical characterization of AA6061 friction stir welded joints using microhardness map [J]. Transactions of Nonferrous Metals Society of China, 2016, 26(9): 2313−2319.

[20] Sato Y S, Urata M, Kokawa H. Parameters controlling microstructure and hardness during friction-stir welding of precipitation-hardenable aluminum alloy 6063 [J]. Metallurgical and Materials Transactions A, 2002, 33(3): 625−635.

[21] Kiral B G, Tabanoglu M, Serindag H T. Finite element modeling of friction stir welding in aluminum alloys joint [J]. Mathematical and Computational Applications, 2013, 18(2): 122−131.

[22] Nandan,R.,Roy,G.G.,Lienert,T.andDebRoy,T.(2007),'Three-dimensionalheat and materialflow during friction stir welding of mild steel', Acta. Mater., 55: 883–95.

[23] Kozlowski PF, Thomas BG, Azzi JA, Wang H.(1992). "Simple constitutive equations for steel at high temperature." Metallurgical and Materials Transactions A, 23(3), pp 903–918.

[24] Zienkiewicz OC and Taylor. R L. (1996). "A Finite Point Method In Computational Mechanics. Applications To Convective Transport And Fluid Flow." International Journal For Numerical Methods in Engineering, 39, pp. 3839-3866.

[25] Zhu XK, Chao YJ. (2004). "Numerical Simulation of transient temperature and residual stresses in friction stir welding of 304L stainless steel." Journal of Material Process and Technology,146, pp.263–272.

[26] Brandes EA, Brook GB (1999). "Smithells metals." reference book, 7th edition, Oxford: Butterworth-Heinemann.

[27] Ayer R, Jin HW, Mueller RR, Ling S, Ford S. (2005). "Interface structure in a Fe–Ni friction stir welded joint." Scripta Materialia, 53, pp.1383–1387.

[28] Carslaw HS, Jaeger JC (1959). "Conduction of heat in solids." 2nd edition. Oxford: Clarendon Press; pp. 87–90.

[29] S.A. Khodir, T. Shibayanagi, Microstructure and Mechanical Properties of Friction Stir Welded Dissimilar Aluminum Joints of AA2024-T3 and AA7075-T6, Material Transaction 48 (2007) 1928–1937.

[30] J.-Q. Su, T. Nelson, R. Mishra, M. Mahoney, Microstructural investigation of friction stir welded 7050-T651 aluminium, Acta Mater. 51 (2003) 713–729.

[31] M.M.Z.Ahmeda,B.P.Wynnea,W.M.Rainfortha,P.L.Threadgill,Microstructure,crystallographictextureandmechanical properties of friction stir welded AA2017A, Mater.Charact. 64 (2012) 107–117.

[32] M.M.Z.Ahmeda,B.P.Wynnea,W.M.Rainfortha,P.L.Threadgill, An investigation of hardness, microstructure andcrystallographic texture in thick sectioned friction stir weldedAA6082, in : 7th International Friction Stir Welding Symposium, Awaji Island, Japan, 2012.

[33] Y.S. Lim, S.H. Kim, K.J. Lee, Effect of residual stress on the mechanical prop-erties of FSW joints with SUS409L, Adv. Mat. Sci. Eng. (2018), 2018.

[34] Hatamleh O, Rivero IV, Swain SE. An investigation of the residual stress characterization and relaxation in peened friction stir welded aluminum–lithium alloy joints. Mater Des 2009;30(9):3367–73.

[35] Richter-Trummer V, Suzano E, Beltrão M, Roos A, Dos SantosJF, De Castro PMST. Influence of the FSW clamping force onthe final distortion and residual stress field. Mater Sci Eng A2012;538:81–8, http://dx.doi.org/10.1016/j.msea.2012.01.016.

[36] Muránskya O, Hamelina CJ, Smithb MC, Bendeicha PJ, Edwardsa L. The effect of plasticity theory on predicted residual stress fields in numerical weld analyses. Comput Mater Sci 2012;54:125–34.

[37] Quested TE, LGreer A. The effect of the size distribution of inoculant particles on as-cast grain size in aluminium alloys. Acta Mater 2004;52:3859–68.

[38] Padmanaban, V. Ratna Kishore, and V. Balusamy, Numerical Simulation of Temperature Distribution and Material Flow During Friction Stir Welding of Dissimilar Aluminum Alloys, Procedia Engineering 97 (2014) 854 – 863.

[39] Chao, Y.J., X. Qi, and W. Tang, Heat Transfer in Friction Stir W elding---Experimental and Numerical Studies. Journal of Manufacturing Science and Engineering, 2003. 125(1): p. 138-145.